Red absorbing cyclometalated Ir(III) diimine photosensitizers competent for hydrogen photocatalysis

*Simon De Kreijger,[†] Olivier Schott,[⊥] Ludovic Troian-Gautier,[†] Emilie Cauët[£], Garry S. Hanan[⊥] and Benjamin Elias[†]**

[†]Université catholique de Louvain (UCLouvain), Institut de la Matière Condensée et des Nanosciences (IMCN), Molecular Chemistry, Materials and Catalysis (MOST), Place Louis Pasteur 1, bte L4.01.02, 1348 Louvain-la-Neuve, Belgium

[⊥]Département de chimie, Université de Montréal, CP 6128, Succ. Centre-Ville, Montréal (Québec) H3C 3J7, Canada

[£] Spectroscopy, Quantum Chemistry and Atmospheric Remote Sensing (CP 160/09), Université libre de Bruxelles, 50 av. F. D. Roosevelt, B-1050 Brussels, Belgium

KEYWORDS : Hydrogen, Iridium, Red absorbing, Photocatalysis.

ABSTRACT: Two new cyclometalated Ir(III) diimine complexes were used as photosensitizers for homogeneous hydrogen evolution reaction (HER). These complexes were characterized by electrochemistry, UV-Vis absorption, time-resolved and steady-state photoluminescence spectroscopy as well as by theoretical methods. The Metal-Ligand to Ligand Charge Transfer (MLLCT) character of their lowest excited state was shown to be competent for efficient H_2 photoproduction in the presence of $[Co(dmgH)_2(py)Cl]$ as the hydrogen evolution catalyst, triethanolamine as sacrificial electron donor and HBF_4 as the proton source. Under optimized experimental conditions, both complexes displayed HER over a period of more than 90 hours, with turn-over numbers reaching up to 11650, 10600 and 174 mol_{H2} mol_{PS}^{-1} under blue, green and red-light irradiation, respectively. Both complexes showed higher stability and efficiency *vs* HER than most of the previously described systems of the same kind.

INTRODUCTION

In the view of developing a new sustainable energy supply as an alternative or complement to fossil fuels, different technologies have been explored for the conversion of sunlight into useful energy sources.[1,2] Among them, a sunlight-triggered hydrogen evolution reaction (HER) appears to be an interesting solution to worldwide consumption of fossil fuels as hydrogen is an energy-dense and carbon-free fuel.[3,4] From a molecular approach, this HER is typically based on photoinduced electron transfer (PET) from a photosensitizer (PS) to a catalytic center, where hydrogen is produced.[5-10] In this context, cobalt macrocyclic complexes represent popular catalysts for homogeneous proton reduction. Cobaloximes are amongst the most studied molecular catalysts due to their ease of synthesis and fairly high activity.[11,12,13] While the development of such efficient homogeneous molecular catalysts has experienced great progress, the elaboration of photostable

photosensitizers with increased visible light absorption properties still remains a challenging part of the HER advancement.[14] Cobaloximes have been associated to various transition metal-based PSs such as Zn(II),[15] Pt(II),[16,17] Ru (II)[18,19,20] and Re (I)[21,22] complexes. More recently, different Ir(III) bis-cyclometalated complexes have been explored as potential candidates to develop stable and robust PSs for HER.[23,24,25,26] These complexes are excellent candidates due to their inherent photophysical and electrochemical tunability coupled to a high photostability.[14] Even though it has been shown that Ir(III) complexes are outperforming archetypal PS such as $[Ru(bpy)_3]^{2+}$ (bpy = 2,2'-bipyridine), they are still suffering from poor visible light absorption properties that typically do not exceed 450 nm.

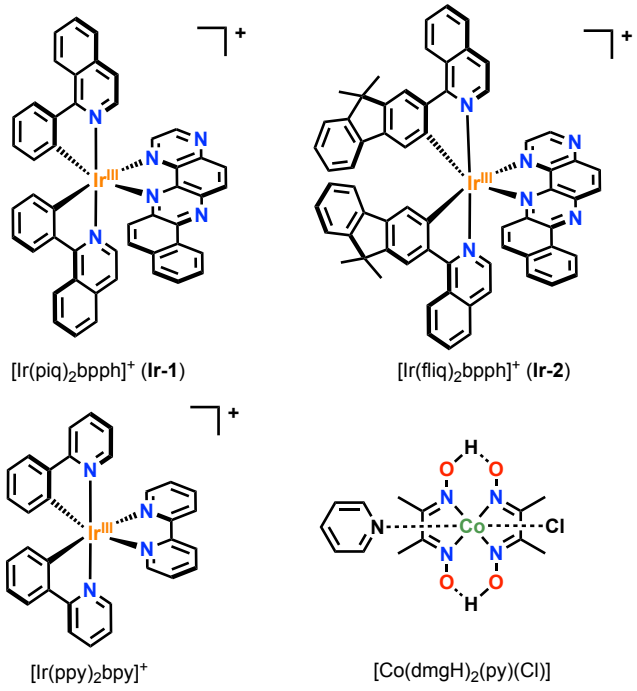

Figure 1. Structures of $[Ir(piq)_2bpph]^+$ (**Ir-1**), $[Ir(fliq)_2bpph]^+$ (**Ir-2**), $[Ir(ppy)_2bpy]^+$ and the precatalyst $[Co(dmgH)_2(py)(Cl)]$ used in this study.

In here, we report two novel Ir(III) based cyclometalated photosensitizers for HER that are efficiently working with [Co(dmgH)$_2$(py)(Cl)] (dmgH$_2$ = dimethylglyoxime) even when red light irradiation is used. These complexes display two cyclometalated **piq** (**Figure 1**, **Ir-1**) or **fliq** (**Figure 1**, **Ir-2**) ligands (**piqH** = 1-phenylisoquinoline; **fliqH** = 1-(9,9-dimethyl-9H-fluoren-2-yl)isoquinoline) and are combined with a recently reported N^N diamine π-extended heteroaromatic ligand, *i.e.* the **bpph** ligand (**bpph** = benzo[*a*]pyrazino[2,3-*h*]phenazine).[27] Strikingly, **Ir-1** and **Ir-2** exhibit a red-shifted absorption up to 620 nm, thus covering most of the visible spectrum. Consequently, both complexes were shown to efficiently evolve hydrogen under blue, green and low energy red-light irradiation, with turn-over numbers up to 11650, 10600 and 174 mol_{H2} mol_{PS}^{-1}, respectively.

RESULTS AND DISCUSSION

Synthesis. First, **fliqH** was obtained from a reported Suzuki coupling reaction between 1-chloroisoquinoline and 2-(9,9-dimethylfluorenyl)boronic acid in the presence of tetrakis(triphenylphosphine)palladium and aqueous sodium carbonate.[28] Second, the iridium dimers (**[Ir(piq)$_2$(μ-Cl)]$_2$** and **[Ir(fliq)$_2$(μ-Cl)]$_2$**) were synthesized according to literature procedures, in which **piqH** or **fliqH** were refluxed in 2-ethoxyethanol/water (3:1) in the presence of iridium trichloride hydrate.[29] The **bpph** ligand was synthesized through a previously described condensation of quinoxaline-5,6-diamine with naphthalene-1,2-dione in acetic acid at 60 °C under microwave irradiation.[27] Finally, **bpph** was chelated onto the Ir(III) dimer precursors (**[Ir(piq)$_2$(μ-Cl)]$_2$** for **Ir-1** and **[Ir(fliq)$_2$(μ-Cl)]$_2$** for **Ir-2**) in ethylene glycol at 110°C (see experimental section). The resulting complexes were further purified by several washing steps with water, ethanol and diethyl ether and were typically obtained with yields greater than 75%.

X-Ray diffraction structures. The slow diffusion of the diisopropylether into acetonitrile solutions of **Ir-1** and **Ir-2** at room temperature led to the growth of crystalline plates suitable for X-Ray diffraction. Both crystals shared the same space group P^{-1}. Crystals were measured at 100 K. Crystallographic and refinement parameters are given in **Table S1**. The quality of data diffraction was good for both structures. The unit cell of **Ir-1** and **Ir-2** included a racemic mixture of the two Λ and Δ enantiomers.

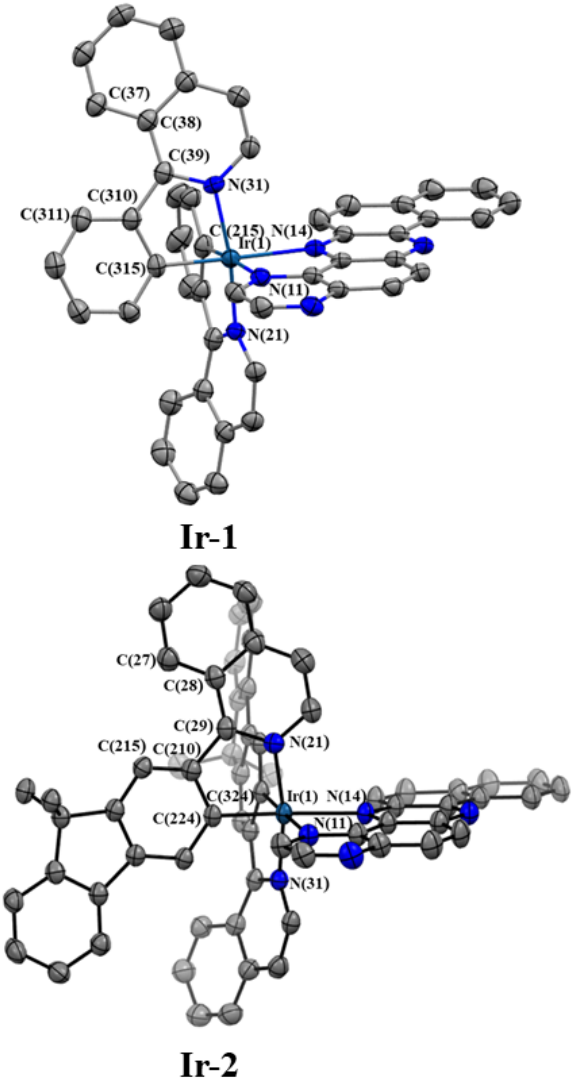

Figure 2. X-Ray structures of the **Ir-1** (top) and **Ir-2** (bottom). Ellipsoids are at the 50 % probability level. H atoms, PF_6^- counter anions, and co-crystallized solvent molecules are omitted for clarity.

The Ir coordination sphere of both photosensitizers exhibited widely similar near octahedral geometries to parent complexes previously reported such as the reference $[Ir(ppy)_2bpy]^+$ or Irpiq-2254tpy or $[Ir(ppyCF_3)_2bbph]^+$ (See **table S2**).[27, 30-31] Deeper in details, the Ir(1)-N(14) bond of the extended conjugated side of **bpph** was 0.1 Å longer than the Ir(1)-N(11) that corresponded to N-bidendate bond lengths in the reference complexes (See **Figure 2** and **table S2**). In the phenylisoquinoline derivatives, a higher typical torsion angle between the cyclometalated ligand and the N-cycle was observed: N(21)-C(29)-C(210)-C(224)= 15.7°(4) for **Ir-2** vs 1.5°(6) in $[Ir(ppy)_2bpy]^+$. The hindered fliq cyclometalated derivative **Ir-2** showed weakly more angular distortions in the coordination sphere than **Ir-1** (See **table S2**).

Electrochemical Characterization. The electrochemical data for **Ir-1** and **Ir-2** were measured by cyclic voltammetry in dry deoxygenated acetonitrile, a suitable solvent for photocatalytic H_2 production, using 0.1M $TBAPF_6$ as supporting electrolyte (**Figure 3**). The half-wave electrochemical potentials are gathered in **Table 1**.

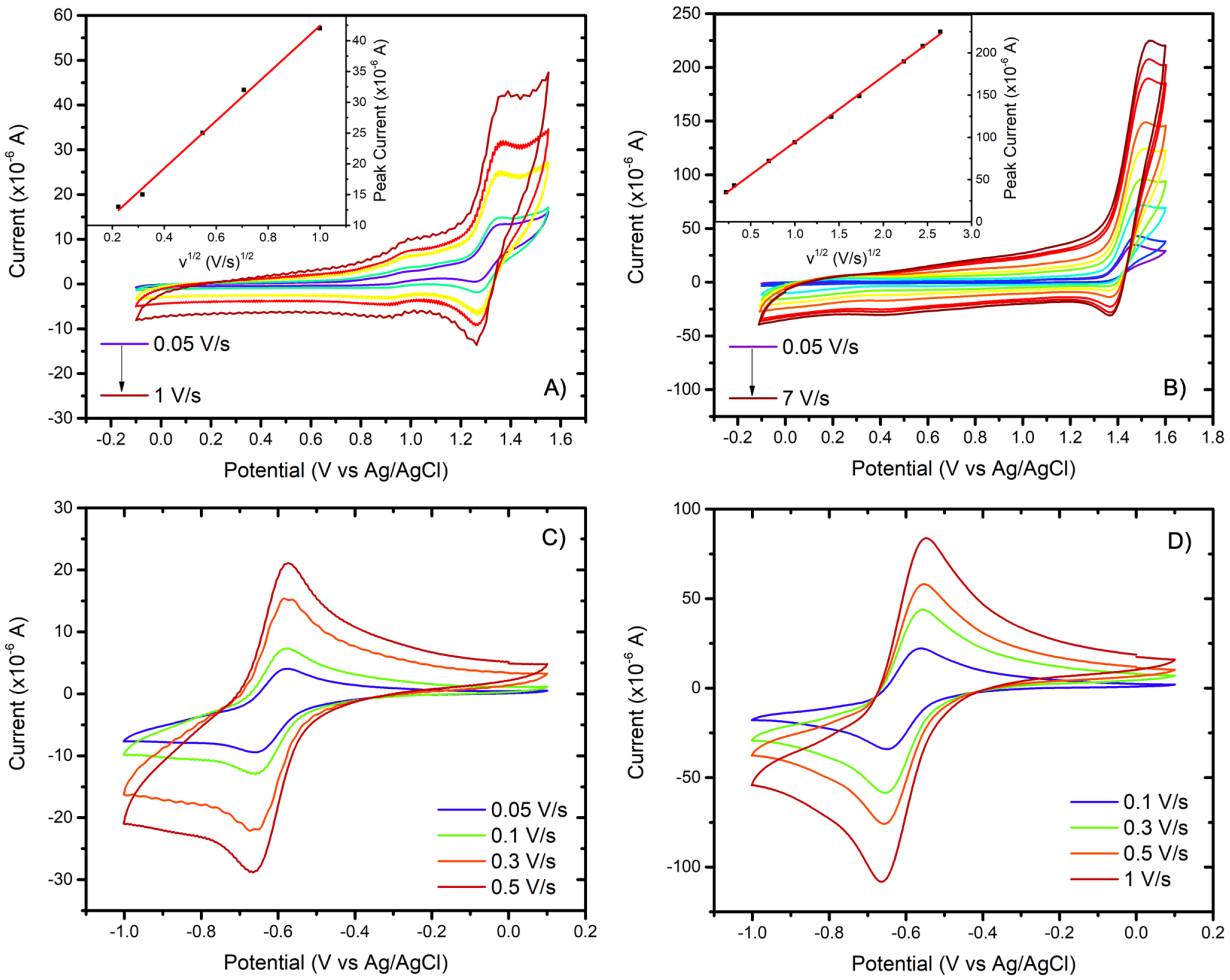

Figure 3. Cyclic voltammograms of **Ir-2** (A-C) and **Ir-1** (B-D) recorded at the indicated scan rate in acetonitrile containing 0.1M $TBAPF_6$. The concentration of **Ir-1** was 1 mM whereas a concentration of 0.5 mM was used for **Ir-2**. The inset of panel A and B shows the dependence of the peak current versus the square root of the scan rate, according to the Randles-Sevcik equation.[32]

Table 1. Electrochemical and photophysical properties of **Ir-1**, **Ir-2** and **$[Ir(ppy)_2bpy]^+$** in acetonitrile at room temperature.

	$[Ir(piq)_2(bpph)]^+$ (Ir-1)	**$[Ir(fliq)_2(bpph)]^+$ (Ir-2)**	**$[Ir(ppy)_2bpy]^+$**
E_{ox}[a]	+ 1.41	+ 1.30;+ 1.62	+ 1.37
E_{red}[a]	–0.60; –1.33; –1.77	–0.61; –1.33; –1.55; –1.74	–1.30
λ_{abs}[b], [c]	300 (482); 340 (317); 428 (140); 455 (109); 560 (11.7); 620 (9.4)	303 (618); 346 (429); 365 (412); 430 (183); 500 (36.6); 560 (10.1); 620 (9.2)	267 (487); 310 (227); 376 (64); 412 (36)
λ_{em}[b], [d]	776	667, 778	599
Φ_{PL}	0.001 [e]	0.002[e]	0.022 [f]
τ (ns)	τ_1 = 19 ns τ_2 = 410 ns	τ_1 = 450 ns τ_2 = 1300 ns	365 ns [g]

[a] Electrochemical data (in V vs Ag/AgCl) were measured with tetrabutylammonium hexafluorophosphate (0.1 M) as supporting electrolyte with a sweep rate of 100 mV s^{-1} and a photosensitizer concentration of 1mM (**Ir-1**) and 0.5

mM (**Ir-2**) [b] In nm, recorded in argon purged acetonitrile. [c] Values in parenthesis indicate the molar absorption coefficient, ε x 10^2 $M^{-1}cm^{-1}$. [d] excitation at 450 nm. [e] Measured *vs*. $[Os(bpy)_3]^{2+}$ (ϕ_{ref} = 0.005 in argon-saturated acetonitrile) (λ_{exc} = 450 nm).[33] [f] Measured under air-equilibrated solution *vs*. Quinine in 0.5M H_2SO_4 in water (ϕ_{ref} = 0.546 - λ_{exc} = 365 nm).[33] [g] from ref [34]

Ir-2 displayed a reversible one-electron oxidation wave, $E_{ox,\,\mathbf{Ir\text{-}2}}$ = + 1.31 V *vs*. Ag/AgCl , that, in agreement with the literature, was assigned to the oxidation of the Ir(III)-cyclometalated ligand fragment.[35] **Ir-1** exhibited an irreversible Ir(III)-cyclometalated ligand oxidation wave at scan rates comprised between 0.05 and 1 V/s. When the scan rate was increased to values larger than 1V/s, reversibility was observed which allowed to determine an oxidation potential, $E_{ox,\,\mathbf{Ir\text{-}1}}$ = + 1.41 V *vs*. Ag/AgCl. In both cases, the dependence of the peak current versus the square root of the scan rate was linear, in agreement with the Randles-Sevcik equation.[32] This implies that the electrochemical reaction is a reversible electron transfer process involving freely diffusing redox species. The slightly less anodic oxidation for **Ir-2** likely originates from the extended π-conjugation on the **fliq** compared to its homologue **Ir-1** containing the **piq** ligand. Furthermore, an additional oxidation process was observed at 1.62 V *vs*. Ag/AgCl for **Ir-2**. This latter was ascribed to the oxidation of the **fliq** moieties. Indeed, an irreversible oxidation process at 1.68 V *vs*. Ag/AgCl was observed for the ligand alone in acetonitrile (**Figure S12**). **Ir-1** and **Ir-2** displayed a similar reversible one-electron reduction pattern, with waves at –0.60 V and –1.33 V *vs*. Ag/AgCl corresponding to a reduction process taking place on the **bpph** ligand as shown for related complexes.[27] Further cathodic electrochemical processes involve both the **bpph** and **fliq** or **piq** ligands.

Theoretical Studies. The excited state of bis-cyclometalated Ir(III) complexes is usually dominated by a mixture of Ligand-Centered (LC), Ligand-to-Ligand Charge Transfer (LLCT), Metal-to-Ligand Charge Transfer (MLCT) and Metal-Ligand-to-Ligand Charge Transfer

(MLLCT) transitions.[14] For **Ir-1** and **Ir-2**, time-dependent density functional theory (TD-DFT) calculations showed that each of these molecular orbital transition contributes to the absorption features (**Figures 4D and 5** and **Figure S13**), with moderate to strong oscillator strength, confirming the CT nature of the lowest excited states. The theoretically determined transitions matched well with the experimentally recorded electronic absorption spectra (**Figure 4D**). Among the most intense transitions of **Ir-1**, the one centered at 328 and 375 nm involved an electronical transition centered on the **bpph** moieties combined with contributions from the Ir(III) center (**Figure 5**). These transitions are hence ascribed to MLLCT transitions. The less energetic contribution to the absorption (457 nm) involved a transition from the metallic center and both ligands towards the **bpph** N^N diimine ligand and is ascribed to a mixture of MLLCT and LLCT transitions. For **Ir-2**, the transitions at 323 and 412 nm are centered on the **bpph** and **fliq** moieties of the complex, respectively, with some contribution from the Ir(III) center. The most bathochromic transition at 467 nm exhibits contributions from both the Ir(III) center and the **bpph** moiety (**Figure 5**). In addition, a clear shift to lower energetical transitions is observed from **Ir-1** to **Ir-2**, confirming the higher stabilization induced by the **fliq** ligand.

Photophysical Characterization. The absorption spectra of ppyH, fliqH, piqH, bbph as well as the absorption and steady-state photoluminescence spectra for **Ir-1** and **Ir-2** were recorded in argon purged acetonitrile at room temperature and are displayed in **Figures 4A-C**. The corresponding photophysical data are gathered in **Table 1** along with those of $[Ir(ppy)_2bpy]^+$, (ppyH = 2-phenylpyridine) for comparison purposes. Both ppyH and piqH exhibited absorption features in the UV region with molar absorption coefficients that ranged from 5000 $M^{-1}cm^{-1}$ (PiqH) to 15,000-20,000 $M^{-1}cm^{-1}$ (ppyH). The phenyl-isoquinoline ligand also presented absorption features between 300 and 350 nm, with moderate molar absorption coefficients. The use of fliqH

allowed to drastically increase the molar absorption coefficient to reach values around 20,000 $M^{-1}cm^{-1}$ at 350 nm. The donor-acceptor structure of the bpph ligand enabled absorption in the visible region with molar absorption coefficients that reached 10,000 $M^{-1}cm^{-1}$ at 410 nm. Regarding the iridium photosensitizers, both **Ir-1** and **Ir-2** are characterized by strong ligand-centered (LC) absorption bands in the UV region ($\varepsilon > 10^4\ M^{-1}\ cm^{-1}$ at wavelengths < 340 nm). In good agreement with the theoretical studies, lower energy (> 350 nm) Metal-Ligand to Ligand Charge Transfer (MLLCT) transitions are observed with a strong intensity ($\varepsilon > 10^4\ M^{-1}\ cm^{-1}$). As expected, in **Ir-1** and **Ir-2**, the higher electronic conjugation within the π-system of the N^N diimine as well as the use of piq and fliq cyclometalated ligands led to a red-shifted absorption accompanied by an important increase in the molar absorption coefficient compared to the reference photosensitizer $[Ir(ppy)_2bpy]^+$. In line with the TD-DFT analysis, **Ir-2** shows a bathochromic shift compared to **Ir-1**, due the presence of π-conjugated **fliq** ligands.[28]

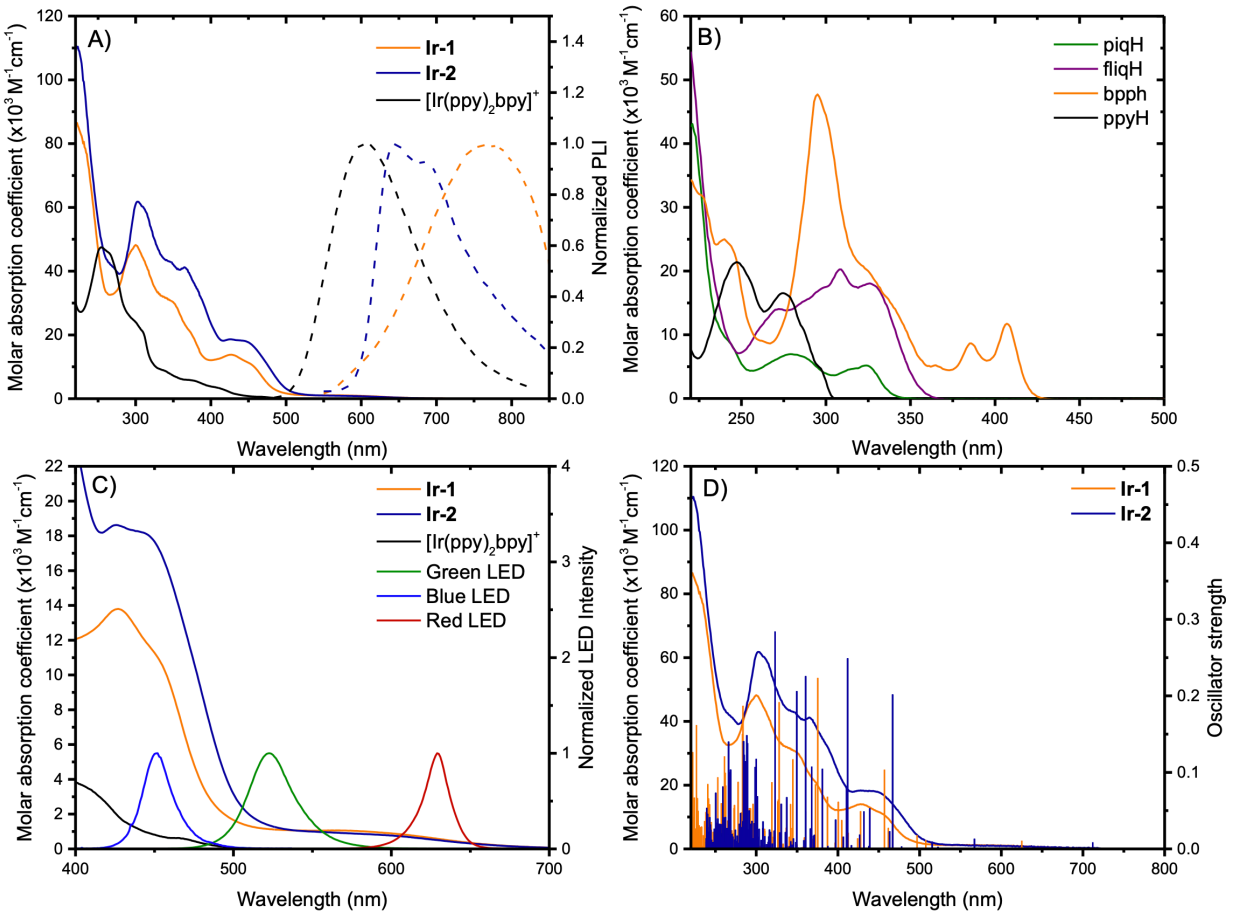

Figure 4. A) Absorption spectra of **Ir-1** (orange)**, Ir-2** (blue) and $[Ir(ppy)_2(bpy)]^+$ (black) recorded in acetonitrile at room temperature as well as the corresponding photoluminescence in argon purged acetonitrile at room temperature. B) Absorption spectra of piqH (green), ppyH (black), fliqH (purple) and bpph (orange) recorded in acetonitrile at room temperature. C) Overlap between the absorption spectra of **Ir-1** (orange)**, Ir-2** (blue) and $[Ir(ppy)_2(bpy)]^+$ (black) and the irradiation source used in this HER study. (D) Absorption spectra of **Ir-1** (orange) and **Ir-2** (blue) recorded in acetonitrile at room temperature with their corresponding calculated TD-DFT transitions in their ground-state singlet geometries. See supporting information for additional details on the theoretical calculations.

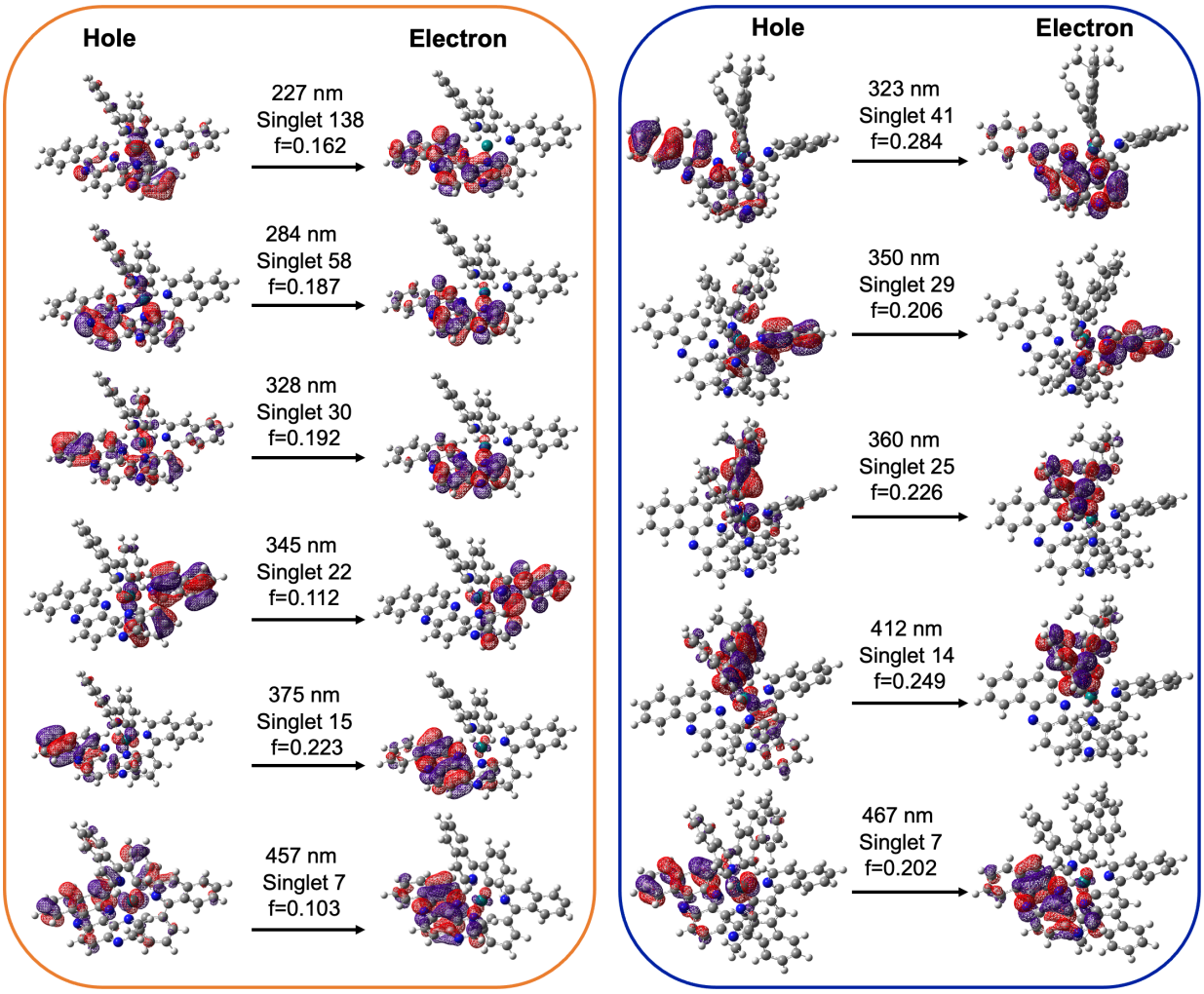

Figure 5. NTOs representation of the indicated transition for **Ir-1** (orange) and **Ir-2** (blue) computed at the B3LYP level of theory. See supporting information for additional details on the theoretical calculations.

Luminescence quantum yields and excited-state lifetimes for the different Ir(III)-based photosensitizers were measured at room temperature in acetonitrile under inert atmosphere (**Table 1**). In air-equilibrated solvents, a decrease in the luminescence intensity with respect to degassed solution is consistently observed for each photosensitizer, indicating a quenching by molecular oxygen.[36] Whereas **Ir-1** and $[Ir(ppy)_2bpy]^+$ exhibit a broad unstructured photoluminescence (**Figure 4A**), as expected for charge transfer (CT) type excited states, a more structured photoluminescence with blue-shifted bands is observed for **Ir-2**. This blue-shifted

photoluminescence arises from a ligand-centered (LC) contribution to the excited state of **Ir-2** in addition to the expected CT-type excited state, as suggested by TD-DFT calculations. The difference between the photoluminescence of $[Ir(ppy)_2bpy]^+$ and the lower-energy lying emission of **Ir-1** and **Ir-2** can be explained by both HOMO and LUMO stabilization due to the π-extended network of the N^N diimine ligand as well as the cyclometalated piq and fliq ligands.

Hydrogen photo-evolution. Driven by their promising photophysical and electrochemical properties, **Ir-1** and **Ir-2** were tested for photocatalytic hydrogen evolution and compared to the prototypical $[Ir(ppy)_2bpy]^+$. $[Co(dmgH)_2(py)(Cl)]$ was used as the pre-catalyst for H_2 production using LED irradiation at different wavelengths, *i.e.* from blue (λ_{max} = 446 nm) to green (λ_{max} = 518 nm) and red (λ_{max} = 634 nm). The duplicated photocatalyzed reactions were carried out in degassed acetonitrile in order to solubilize the Ir(III) complexes with 1M TEOA as sacrificial electron donor and 0.1 M of HBF_4 as proton source. The cobalt catalyst was used in large excess (1 $x10^{-3}$ M) compared to the photosensitizers (5 $x10^{-6}$ M under blue and green light irradiation, and 1 $x10^{-4}$ M under red light irradiation) in order to assess the efficiency and durability of the Ir(III) complexes *vs*. HERs. In addition, four equivalents of $dmgH_2$ (4 $x10^{-3}$ M) were also introduced at the start of the photocatalytic experiments to ensure Co catalyst recovery. Control experiments in the absence of cobalt catalysts did not show any sign of hydrogen photoproduction. Hydrogen evolution was monitored for 12 hours before affirming that no hydrogen was detected. We determined the limit of detection of the instrument at around 0.05 μLH_2 min^{-1}, that corresponds to 82 $mmolH_2.mol^{-1}PS.min^{-1}$ of TOF for a photosensitizer at 0.005 mM in the usual experimental condition of this study.

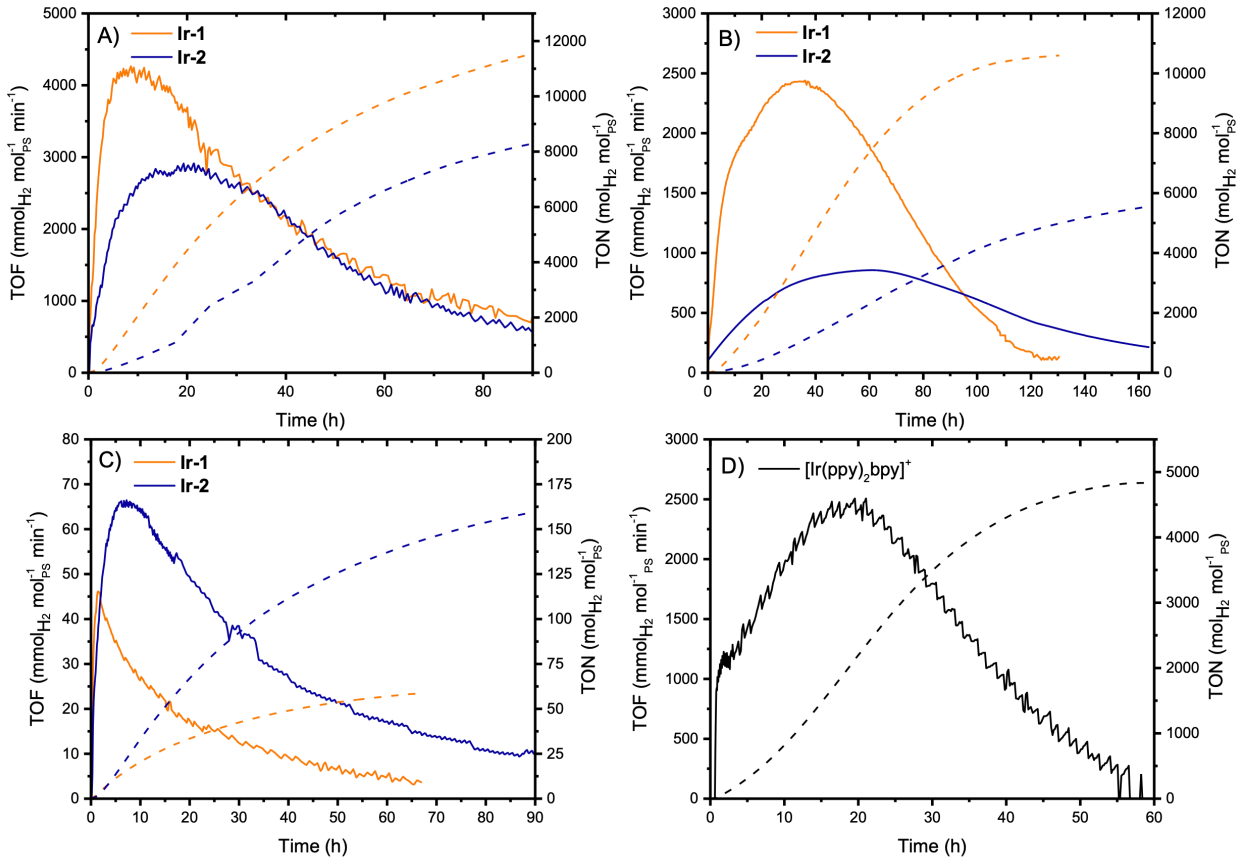

Figure 6. HER at (A) 446 nm with 5 x10^{-6} M Ir(III) photosensitizers, (B) 518 nm with 5 x10^{-6} M Ir(III) photosensitizers, (C) 634 nm of 1 x10^{-4} M Ir(III) c photosensitizers and (D) 446 nm with 5 x10^{-6} M [Ir(ppy)$_2$bpy]$^+$. All experiments were carried out with 1 x10^{-3} M of [Co(dmgH)$_2$(py)(Cl)] and 4 x10^{-3} M dmgH$_2$ in CH$_3$CN with 1 M TEOA as the electron source and 0.1 M HBF$_4$ as the proton source: solid lines, TOF; dashed lines, TON.

Under blue irradiation (**Figure 6 A**), all photosensitizers efficiently achieved the photo-redox process for hydrogen evolution. The reference system [Ir(ppy)$_2$bpy]$^+$/[Co(dmgH)$_2$(py)(Cl)] slowly reached a TOF$_{max}$ of 2480 mmol$_{H2}$ mol^{-1} min^{-1}, followed by a slow decrease to reach a TON of 4850 in 52.9h (**Figure 6D** and **Table 2**). Interestingly, both **Ir-1** and **Ir-2** behaved very differently than the reference system. Indeed, they reacted slowly under blue irradiation to reach a TOFs$_{max}$ of 4250 and 2850 mmol$_{H2}$ mol^{-1} min^{-1}, respectively, followed by a slower decrease compared to [Ir(ppy)$_2$bpy]$^+$, with TONs of 11650 and 8370 in 92.6h, respectively. These systems are clearly outperforming the [Ir(ppy)$_2$bpy]$^+$ based system and most of the systems described in

the literature (**Table 2,** entries 9 to 14) due to their higher TON and longer operating time. Moreover, after 92h of blue light irradiation of **Ir-2** alone in acetonitrile (λ_{max} = 446 nm), its absorption spectrum displays only minor changes, suggesting a high photostability for this photosensitizer. In contrast, the continuous blue irradiation of **Ir-1** showed an increase of the absorbance in the UV region (see figures **S16-17**). Although this strongly suggests a photo-dechelation of the **bpph** ligand, inducing a higher absorbance in the LC region, HER for **Ir-1** is monitored with a higher efficiency compared to **Ir-2**, clearly demonstrating the great potential of this photosensitizer. Control experiments highlighted that the **bpph** ligand was unable to produce hydrogen catalytically (**Table 2, Entry 8**). We also observed that the TOF, and to a lesser extend the TON, decreased when the amount of photosensitizer was doubled ($1x10^{-5}$ M). This indicates that more diluted solutions lead to more efficient hydrogen production, probably by preventing side reactions between photosensitizers in their reduced or excited states. In these conditions, doubling the concentration of HBF_4 (0.2M) did not significantly impact the TOF or TON, indicating that the proton source is not the limiting factor (**Figure S15**). Some catalytic activity could be recovered when a fresh aliquot of photosensitizer was added after 90-114 hours of illumination, indicating that some photosensitizer degradation occurred after such prolonged irradiation and catalysis. Importantly, these results indicate that the four additional $dmgH_2$ equivalents that are added at the start of the experiment help ensure the integrity of the cobaloxime catalyst over time.

Under green light irradiation, the reference system $[Ir(ppy)_2bpy]^+$/$[Co(dmgH)_2(py)(Cl)]$ did not lead to any hydrogen photoproduction. This can be explained by the limited overlap of the absorption spectrum of $[Ir(ppy)_2bpy]^+$ with the spectral profile of the green LED (see **Figure 4C**). **Ir-1** and **Ir-2** are less efficient under green light than under blue light irradiation but still exhibit a

remarkably high activity (**Figure 4B**) compared to other molecular PSs described in the literature (**Table 2,** entries **10** to **12**). Indeed, **Ir-1** and **Ir-2** gradually achieve $TOFs_{max}$ of 2450 and 850 $mmol_{H2}$ mol^{-1} min^{-1}, respectively. This was followed by a slower decrease than under blue light irradiation, meaning that systems are deactivated at a slower rate under less energetic irradiation. The final TONs obtained were 10600 and 5550 in 132.1 and 164.0h, respectively, showing the good efficiency of these novel photosensitizers to photo-evolve H_2 under less energetic irradiation.

Finally, both photosensitizers were also able to perform HER under red light irradiation (**Figure 4C**). In this case, the concentration of both photosensitizers was increased to 10^{-4} M to maximize absorption at these less energetic wavelengths. As the overlap of the absorption spectrum and the emission spectrum of the LED is smaller than for green light, the activity of the complexes was lower than for the previous measurements. Yet, considerable H_2 photoproduction could be detected, with $TOFs_{max}$ of 46 and 66 $mmol_{H2}$ mol^{-1} min^{-1} for **Ir-1** and **Ir-2**, respectively. Then, the activity decreased until the photosensitizers reached a TON of 58 and 173 after 67.0 and 133.1 hours. It is worth mentioning that the **fliq** based photosensitizer showed a better activity under red light irradiation than the **piq** homologue. These results were in the same range of TON and TOF_{max} than a previously reported system (**Table 2,** entries **10** and **11**). It is important to note that the concentration used for hydrogen production using red light irradiation are higher than when blue or green light is used, *i.e.* $1x10^{-4}$ M compared to $5x10^{-6}$ M. This may lead to additional side reaction that could account for the different trend observed between **Ir-1** and **Ir-2** under red light irradiation. The absolute quantum yields for hydrogen production were 0,087 for the reference $[Ir(ppy)_2bpy]^+$ under blue irradiation, 0.13, 0.086 and 0.018 % for **Ir-1**, and 0.097, 0.036 and 0.028 % for **Ir-2** under blue, green and red light irradiation, respectively (**Table S6**).

Again, under red light irradiation, the reference system $[Ir(ppy)_2bpy]^+$/$[Co(dmgH)_2(py)(Cl)]$ did not lead to any hydrogen photoproduction, most probably due to the lack of overlap between the absorption spectrum of $[Ir(ppy)_2bpy]^+$ with the spectral profile of the red LED (**Figure 4C**).

Table 2. Performances for HER of photocatalytic systems under various irradiation wavelengths and comparison of HER efficiency using metal-based complexes as photosensitizer and cobaloxime as the proton reduction catalyst.

	PS[a]	Catalysts	Solvent	SED/H^+	Irr.	TON (vs. PS)[b]	Ref
1	**Ir-1** (5×10^{-6} M and 10^{-4} M for 634 nm irradiation)	$[Co(dmgH)_2(py)(Cl)]$ (10^{-3} M) $dmgH_2$ (4×10^{-3}M)	CH_3CN	TEOA (1 M) HBF_4 (0.1 M)	446 nm 518 nm 634 nm	11650 (92.6h) 10600 (132.1h) 58 (67.0h)	/
2	**Ir-2** (5×10^{-6} M and 10^{-4} M for 634 nm irradiation)	$[Co(dmgH)_2(py)(Cl)]$ (10^{-3} M) $dmgH_2$ (4×10^{-3}M)	CH_3CN	TEOA (1 M) HBF_4 (0.1 M)	446 nm 518 nm 634 nm	8370 (92.6h) 5550 (164.0h) 174 (133.1h)	/
3	$[Ir(ppy)_2bpy]^+$ (5×10^{-6} M)	$[Co(dmgH)_2(py)(Cl)]$ (10^{-3} M) $dmgH_2$ (4×10^{-3}M)	CH_3CN	TEOA (1 M) HBF_4 (0.10 M)	446 nm 518 nm 634 nm	4850 (52.9h) No H_2 detected No H_2 detected	/
4	**Ir-1** (1×10^{-5} M)	No catalyst	CH_3CN	TEOA (1 M) HBF_4 (0.1 M)	446 nm	No H_2 detected	
5	**Ir-2** (1×10^{-5} M)	No catalyst	CH_3CN	TEOA (1 M) HBF_4 (0.1 M)	446 nm	No H_2 detected	
6	**Ir-1** (1×10^{-5} M), **bpph** (1×10^{-4} M)	$Co(BF_4)_2.6H_2O$ (1×10^{-3} M)	CH_3CN	TEOA (1 M) HBF_4 (0.1 M)	446 nm	No H_2 detected	
7	**Ir-1** (1×10^{-5} M),	$Co(BF_4)_2.6H_2O$ (1×10^{-3} M)	CH_3CN	TEOA (1 M) HBF_4 (0.1 M)	446 nm	No H_2 detected	
8	**bpph** (1×10^{-4} M),	$[Co(dmgH)_2(py)(Cl)]$ (10^{-3} M) $dmgH_2$ (4×10^{-3}M)	CH_3CN	TEOA (1 M) HBF_4 (0.1 M)	446 nm	No H_2 detected	
9	$[Ir(ttbutpy)(btfp)Cl]^+$ (20 mM)	$[Co(dmgH_2)(4\text{-}COOMe\text{-}py)Cl]$ (335 mM)	CH_3CN	AscNa (100 mM) Acetate buffer	>390 nm	670 (3h)	[25]
10	$[Ir(piq)_2\text{-}L(tpy)\text{-}Co]$ (0.1 M)	Dyad	CH_3CN	TEOA (0.5 M) HBF_4 (0.05 M)	452 nm 525 nm 630 nm	180 (2.3h) 251 (3h) 80 (110h)	[24]
11	$[Ru(Tolyltpy)(L1)]^{2+}$ (0.1 mM)	$[Co(H_2O)_6](BF_4)_2$ (1 mM) $dmgH_2$ (6 mM)	DMF	TEOA (1.0 M) HBF_4 (0.1M)	445 nm 630 nm	269 (24h) 135 (60h)	[37]
12	$[Ir(4'\text{-}Py\text{-}tpy)(4'\text{-}MeO\text{-}tppy)\text{-}Co]^+$ (0.1 mM)	Dyad	CH_3CN	TEOA (1.0 M) HBF_4(0.1 M)	452 nm 525 nm	440 (66h) 113 (25h)	[26]
13	$[ZnTMPyP]^{4+}$ (4.0×10^{-5} M)	$[Co(dmgH)_2(py)(Cl)]$ (4.9×10^{-4} M)	CH_3CN H_2O	TEOA (5% (v/v) H_2O	> 440 nm	280 (20h)	[15]
14	$[Ir(NBI)_2phen]^+$ (2.2×10^{-4} M)	$[Co(dmgH)_2(py)(Cl)]$ (3.7×10^{-4} M)	CH_3CN H_2O	DMT (0.07 M) H_2O	452 nm	372 (20h)	[23]

[a] The abbreviations used for the different ligands correspond to: ttbutpy = 4,4',4"-tri-*tert*-butyl-2,2':6',2"-terpyridine, btfp = 2-(benzo[b]thiophen-2-yl)-5-trifluoromethylpyridine, L(tpy) = 2,2';5',4"-terpyridine, Tolyltpy = 4'-tolyl-2,2':6',2"-terpyridine, L1 = 6-(4-Bromophenyl)-2,4-di(pyridin-2-yl) pyrimidine, 4'-Py-tpy = 4'-(4-

pyridinyl)-2,2';6',2"-terpyridine, 4'-MeO)tppy = 2,6-diphenyl-4-(4'-methoxyphenyl)pyridine, $[ZnTMPyP]^{4+}$ = zinc *meso*-tetrakis(1-methyl-pyridinium-4-yl)porphyrin, NBI = 1,8-naphthalenebenzimidazole, phen = 1,10-phenanthroline. [b] TON in mol_{H2} mol_{PS}^{-1}. For **Ir-1**, **Ir-2** and $[Ir(ppy)bpy]^+$ the error associated for the TON values is estimated as 10%.

Mechanistic considerations. The results presented herein point toward a mechanism that involves electron transfer from triethanolamine to the excited-state photosensitizers. Stern-Volmer experiments were carried out in argon purged acetonitrile with $[Ir(ppy)_2bpy]^+$, **Ir-1** and **Ir-2**. The addition of triethanolamine to argon-purged solutions of Ir(III) photosensitizers led to a decrease in steady-state photoluminescence (**Figure S18**). However, the corresponding Stern-Volmer plots were non-linear, with downward curvature, preventing the accurate determination of quenching rate constants.

From the excited-state PL spectra and the electrochemical measurements, excited-state reduction potential $E_{1/2}Ir^{(III*/II)}$ of 1.67 and 1.66 V vs NHE were calculated for **Ir-1** and **Ir-2**, respectively. With those potential, a driving force for electron transfer from TEOA (E° = 1.08 V vs NHE) to the photosensitizers' excited state of –0.59 and –0.58 eV was estimated for **Ir-1** and **Ir-2**, respectively. The driving force for electron transfer from the excited photosensitizer to the cobalt pre-catalyst was only slightly exothermic. Hence, giving the large concentration of TEOA used herein as well as the favorable driving force for electron transfer, the proposed mechanism would be more consistent with electron transfer from TEOA to the excited-state PS, which would then transfer an electron to the cobaloxime.[38] The second electron transfer event to generate the active Co(I) catalyst would in all cases be energetically uphill, pointing towards an alternative mechanism for H_2 evolution via disproportionation of Co(II) to Co(III) and Co(I).[11, 13, 39]

To gain additional mechanistic information and assess if excited-state electron transfer is occurring between the excited photosensitizers and triethanolamine, photolysis experiments with **Ir-1** and **Ir-2** in the presence of 0.1 M TEOA were performed in argon-purged acetonitrile. In both

cases, photolysis using blue LED irradiation led to spectral changes with novel absorption features centered around 370 nm and 470 nm. These spectral changes were in agreement with the formation of the monoreduced Ir(III) photosensitizers, as observed by transient absorption spectroscopy for related photosensitizers.[27, 40-41] Interestingly, the reaction proceeded faster for **Ir-1** compared to **Ir-2**, that was still undergoing reaction after 20 minutes of irradiation (**Figure 7**). The initial state of the photosensitizers could then be recovered by the addition of potassium persulfate, a known sacrificial oxidant. However, as indicated by the dashed lines in **Figure 7**, the initial photosensitizer was not fully regenerated, presumably indicating some degradation of the accumulated reduced photosensitizer over time. This degradation could also occur within the hydrogen evolution reaction, although we hypothesize that the monoreduced photosensitizer is not accumulated over long periods of time as it would react with the cobalt catalyst.

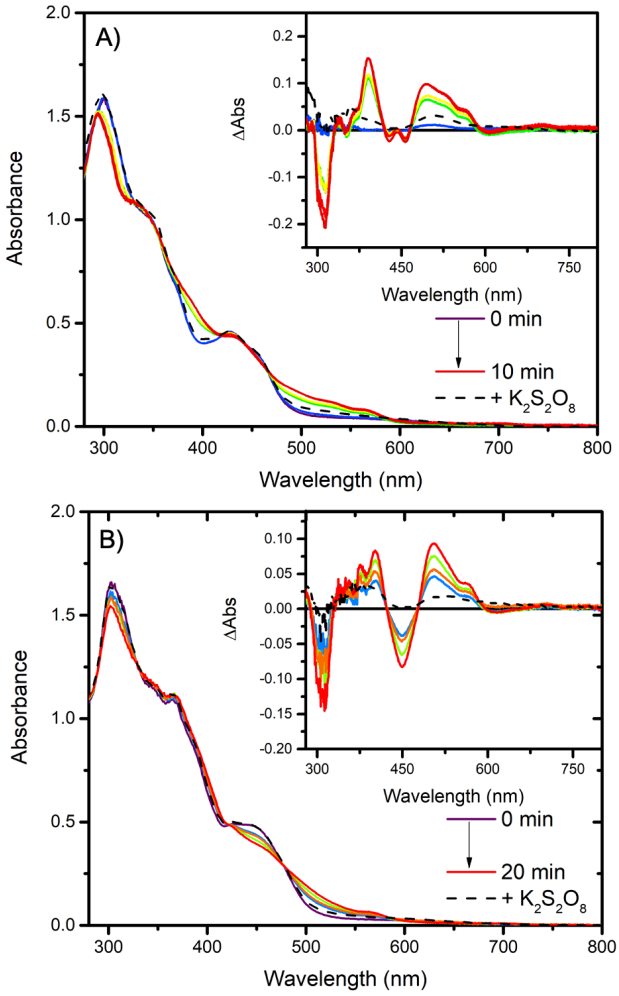

Figure 7. Absorption spectra of **Ir-1** (A) and **Ir-2** (B) recorded in argon-purged acetonitrile at room temperature over time following irradiation with blue LED light in the presence of 0.1 M TEOA. After the irradiation, an excess of $K_2S_2O_8$ was added to oxidize the photo-reduced photosensitizer and investigate reversibility.

CONCLUSIONS

The synthesis of two novel Ir(III) photosensitizers and their efficiency for the visible light mediated hydrogen production reaction was reported. The ground and excited-state behavior of both photosensitizers were fully characterized. Red-shifted absorption properties were obtained by the judicious use of cyclometalating **piq** and **fliq** ligand in combination with the recently reported **bpph** N^N diimine ligand. The absorption properties were fully in line with theoretical

calculations and ascribed the red-shifted transitions from both the Ir(III) center and the **bpph** moiety. In acetonitrile, in the presence of a cobalt catalyst, a sacrificial electron donor and a proton source, both Ir(III) photosensitizers were able to utilize blue, green and red photons to generate hydrogen with turn-over numbers up to 11650, 10600 and 174 mol_{H2} mol_{PS}^{-1}, respectively, outperforming most the parent compounds described in the literature.

EXPERIMENTAL SECTION

Ethanol (≥99.9%, VWR), dichloromethane (≥99.9%, VWR), methanol (≥99.9%, VWR), tetrahydrofuran (≥99.9%, VWR), diethyl ether (≥99%, VWR), n-hexane (≥97%, VWR), ethyl acetate (≥99.9%, VWR), petroleum ether 40-60°C (VWR), 2-ethoxyethanol (≥99%, Acros Organics), ethylene glycol (≥99%, Roth), acetonitrile (≥99.9%, VWR), acetic acid glacial (≥99.9%, VWR), $[NH_4][PF_6]$ (99%, Fluorochem), SiO_2 (40-63 mm, Rocc), Celite (Roth), 4-nitro-*o*-phenylenediamine (98%, Acros Organics), glyoxal 40 wt. % solution in water (Acros Organics), hydroxylamine hydrochloride (≥99%, Acros Organics), palladium (10%) on activated carbon (Chimet), hydrazine monohydrate (hydrazine 64%) (≥99.9%, Acros Organics), 2-naphtoquinone (97% Sigma Aldrich), 2-iodo-9,9-dimetylfluorene ((≥98%, TCI), *n*-butyllithium 1.6M solution in hexanes (Acros Organics), Trimethyl borate (99%, Acros Organics), 1-chloroisoquinoline (97%, Fluorochem), Triphenylphosphine (99%, Sigma Aldrich), sodium carbonate (99.5%, Acros Organics), iridium trichloride hydrate (53% Ir, Pressure Chemical), 1-phenylisoquinoline (98% TCI) were purchased from commercial sources and used as received. $[Pd(PPh_3)_4]$,[42] $[Os(bpy)_3](PF_6)_2$,[43] $[Co(dmgH)_2(py)(Cl)]$,[38] (9,9-dimethyl-9*H*-fluoren-2-yl)boronic acid, 1-(9,9-dimethyl-9H-fluoren-2-yl)isoquinoline (**FliqH**),[28] Benzo[*a*]pyrazino[2,3-*h*]phenazine (**bpph**)[27] and $[Ir(piq)_2(\mu\text{-}Cl)]_2$,[29] were synthesized according to published procedures. Water was purified by

a Millipore Milli-Q system. The precipitates were isolated by centrifugation at 4000 rpm for 3 min in a Hettich Universal 320 centrifuge. Microwave synthesis, nuclear magnetic resonance, mass spectrometry, UV-visible spectroscopy, fluorescence spectroscopy and the set-up for gas chromatography[24] are further described in the Supporting Information.

$[Ir(fliq)_2(\mu\text{-}Cl)]_2$. Iridium trichloride hydrate (75 mg, 0.214 mmol, 1 eq.) and 1-(9,9-dimethyl-9H-fluoren-2-yl)isoquinoline (150 mg, 0.467 mmol, 2.2 eq.) were dissolved in a mixture of 2-ethoxyethanol (3 ml) and water (1 ml). The mixture was then heated at reflux overnight under argon atmosphere. The solution was allowed to cool down at room temperature, and water (10 ml) was added. The deep red precipitate was centrifugated, washed with water and diethyl ether, and then dried under vacuum. The dimeric precursor **$[Ir(fliq)_2(\mu\text{-}Cl)]_2$** was isolated as a red powder (119 mg, 0.068 mmol, 64%). ^{1}H NMR (500 MHz, $CDCl_3$) δ 9.10 (d, *J* = 6.3 Hz, 4H), 9.02 (d, *J* = 8.4 Hz, 4H), 8.18 (s, 4H), 7.96 (d, *J* = 7.6 Hz, 4H), 7.92 – 7.88 (m, 4H), 7.83 (ddd, *J* = 8.3, 6.9, 1.4 Hz, 4H), 7.22 (d, *J* = 7.3 Hz, 4H), 7.08 (td, *J* = 7.3, 1.1 Hz, 4H), 6.97 (td, *J* = 7.5, 0.9 Hz, 4H), 6.89 (d, *J* = 7.5 Hz, 4H) 6.62 (d, *J* = 6.2 Hz, 4H), 6.46 (s, 4H), 1.39 (s, 12 H), 1.38 (s, 12 H).

$[Ir(piq)_2(bpph)]^+$. $[Ir(piq)_2(\mu\text{-}Cl)]_2$ (40 mg, 0.031 mmol, 1 eq.) and **bpph** (18.6 mg, 0.066 mmol, 2.1 eq.) were dissolved in 4 mL of ethylene glycol. The mixture was then heated at 110°C for 18 hours under argon atmosphere. The solution was then allowed to cool down at room temperature and 5 mL of a NH_4PF_6 saturated aqueous solution were added. The dark precipitate was centrifugated and washed with water (three times), ethanol (two times) and sorely with diethyl ether (five to eight times). The iridium complex was isolated as a dark green powder (49 mg, 0.047 mmol, 76%). ^{1}H NMR (500 MHz, CD_3CN) δ 9.53 – 9.46 (m, 1H), 9.12 (d, *J* = 2.6 Hz, 1H), 9.07 (m, 1H), 9.01 – 8.96 (m, 1H), 8.83 (d, *J* = 9.4 Hz, 1H), 8.63 (d, *J* = 9.4 Hz, 1H), 8.48 (m, 2H), 8.04

(d, *J* = 2.6 Hz, 1H), 7.99 – 7.74 (m, 11H), 7.54 (d, *J* = 6.5 Hz, 1H), 7.27 (m, 2H), 7.23 – 7.13 (m, 3H), 7.02 (m, 2H), 6.39 (dd, *J* = 7.7, 1.3 Hz, 1H), 6.32 (dd, *J* = 7.7, 1.3 Hz, 1H). HRMS(ESI) m/z calculated for $[C_{48}H_{30}N_6{}^{191}Ir\text{-}PF_6]^+$ = 881.21324; found 881.21326.

$[Ir(fliq)_2(bpph)]^+$. $[Ir(fliq)_2(\mu\text{-}Cl)]_2$ (48 mg, 0.027 mmol, 1 eq.) and **bpph** (18.6 mg, 0.058 mmol, 2.1 eq.) were dissolved in 4 mL of ethylene glycol. The mixture was then heated at 110°C for 18 hours under argon atmosphere. The solution was then allowed to cool down at room temperature and 5 mL of a NH_4PF_6 saturated aqueous solution were added. The dark precipitate was centrifugated and washed with water (three times), ethanol (two times) and sorely with diethyl ether (five to eight times). The iridium complex was isolated as a dark green powder (55mg, 0.043 mmol, 79%). ^{1}H NMR (500 MHz, CD_3CN) δ 9.49 (d, *J* = 8.1 Hz, 1H), 9.14 – 9.09 (m, 2H), 9.02 (d, *J* = 8.4 Hz, 1H), 8.84 (d, *J* = 9.4 Hz, 1H), 8.64 (d, *J* = 9.4 Hz, 1H), 8.60 (s, 1H), 8.55 (s, 1H) 8.15 (d, *J* = 2.7 Hz, 1H), 8.00 – 7.80 (m, 10H), 7.77 (d, *J* = 9.6 Hz, 1H), 7.63 (d, *J* = 9.6 Hz, 1H), 7.56 (d, *J* = 6.5 Hz, 1H), 7.55 – 7.50 (m, 2H), 7.32 – 7.27 (m, 3H), 7.22 (m, 2H), 7.13 (td, *J* = 7.5, 1.1 Hz, 1H), 7.10 (td, *J* = 7.5, 1.1 Hz 1H) 7.01 (m, 1H), 6.87 – 6.84 (m, 1H), 6.70 – 6.65 (m, 2H), 1.72 (s, 3H), 1.63 (s, 3H), 1.57 (s, 6H). HRMS(ESI) m/z calculated for $[C_{66}H_{46}N_6{}^{191}Ir\text{-}PF_6]^+$ = 1113.33844; found 1113.33862.

ASSOCIATED CONTENT

Supporting Information. Experimental, Characterization, Electrochemistry, X-Ray crystallography, TD-DFT Calculations, LED Emission Profiles, Photostability Measurements. This material is available free of charge on the ACS Publications website

AUTHOR INFORMATION

Corresponding Author

benjamin.elias@uclouvain.be

Author Contributions

The manuscript was written through contributions of all authors. All authors have given approval to the final version of the manuscript.

Funding Sources

No competing financial interests have been declared.

ACKNOWLEDGMENT

S.D.K. and B.E. gratefully acknowledge the UCLouvain for financial support. L. T.-G. is a Collaborateur Scientifique of the Fonds de la Recherche Scientifique – FNRS. Computational resources have been provided by the Shared ICT Services Centre, Université Libre de Bruxelles. G.S.H. thanks the Natural Sciences and Engineering Research Council (NSERC) of Canada for financial support. O.S. thanks the Fonds de Recherche du Québec Nature et Technologie for Phd fellowship and the ESP of Université de Montréal for the J. Armand Bombardier fellowship.

REFERENCES

1. Nocera, D. G., Chemistry of Personalized Solar Energy. *Inorg. Chem.* **2009,** *48*, 10001-10017.
2. Armaroli, N.; Balzani, V., Solar Electricity and Solar Fuels: Status and Perspectives in the Context of the Energy Transition. *Chem-Eur. J.* **2016,** *22*, 32-57.
3. Graetz, J., New approaches to hydrogen storage. *Chem. Soc. Rev.* **2009,** *38*, 73-82.
4. Bolton, J. R., Solar photoproduction of hydrogen: A review. *Sol. Energy* **1996,** *57*, 37-50.
5. Ozawa, H.; Haga, M.-a.; Sakai, K., A Photo-Hydrogen-Evolving Molecular Device Driving Visible-Light-Induced EDTA-Reduction of Water into Molecular Hydrogen. *J. Am. Chem. Soc.* **2006,** *128*, 4926-4927.
6. Yatsuzuka, K.; Yamauchi, K.; Sakai, K., Redox tuning in Pt(bpy)-viologen catalyst-acceptor dyads enabling photocatalytic hydrogen evolution from water. *Chem. Commun.* **2021,** *57*, 5183-5186.

7. Yatsuzuka, K.; Yamauchi, K.; Kawano, K.; Ozawa, H.; Sakai, K., Improving the overall performance of photochemical H2 evolution catalyzed by the Co-NHC complex via the redox tuning of electron relays. *Sustainable Energy Fuels* **2021,** *5*, 740-749.
8. Lang, P.; Habermehl, J.; Troyanov, S. I.; Rau, S.; Schwalbe, M., Photocatalytic Generation of Hydrogen Using Dinuclear π-Extended Porphyrin–Platinum Compounds. *Chem-Eur. J.* **2018,** *24*, 3225-3233.
9. Habermehl, J.; Nauroozi, D.; Martynow, M.; Vilk, Y. E.; Beranek, R.; Guthmuller, J.; Rau, S., Synthesis and hydrogen evolving catalysis of a panchromatic photochemical molecular device. *Sustainable Energy Fuels* **2020,** *4*, 619-624.
10. Teets, T. S.; Nocera, D. G., Photocatalytic hydrogen production. *Chem. Commun.* **2011,** *47*, 9268-9274.
11. Artero, V.; Chavarot-Kerlidou, M.; Fontecave, M., Splitting Water with Cobalt. *Angew. Chem. Int. Ed.* **2011,** *50*, 7238-7266.
12. Connolly, P.; Espenson, J. H., Cobalt-catalyzed evolution of molecular hydrogen. *Inorg. Chem.* **1986,** *25*, 2684-2688.
13. Dempsey, J. L.; Brunschwig, B. S.; Winkler, J. R.; Gray, H. B., Hydrogen Evolution Catalyzed by Cobaloximes. *Acc. Chem. Res.* **2009,** *42*, 1995-2004.
14. Bevernaegie, R.; Wehlin, S. A. M.; Elias, B.; Troian-Gautier, L., A Roadmap Towards Visible Light Mediated Electron Transfer Chemistry with Iridium(III) Complexes. *ChemPhotoChem* **2021,** *5*, 217-234.
15. Lazarides, T.; Delor, M.; Sazanovich, I. V.; McCormick, T. M.; Georgakaki, I.; Charalambidis, G.; Weinstein, J. A.; Coutsolelos, A. G., Photocatalytic hydrogen production from a noble metal free system based on a water soluble porphyrin derivative and a cobaloxime catalyst. *Chem. Commun.* **2014,** *50*, 521-523.
16. Du, P.; Schneider, J.; Jarosz, P.; Zhang, J.; Brennessel, W. W.; Eisenberg, R., Photoinduced Electron Transfer in Platinum(II) Terpyridyl Acetylide Chromophores: Reductive and Oxidative Quenching and Hydrogen Production. *J. Phys. Chem. B* **2007,** *111*, 6887-6894.
17. Wang, X.; Goeb, S.; Ji, Z.; Pogulaichenko, N. A.; Castellano, F. N., Homogeneous Photocatalytic Hydrogen Production Using π-Conjugated Platinum(II) Arylacetylide Sensitizers. *Inorg. Chem.* **2011,** *50*, 705-707.
18. Fihri, A.; Artero, V.; Razavet, M.; Baffert, C.; Leibl, W.; Fontecave, M., Cobaloxime-Based Photocatalytic Devices for Hydrogen Production. *Angew. Chem. Int. Ed.* **2007,** *47*, 564-567.
19. Li, C.; Wang, M.; Pan, J.; Zhang, P.; Zhang, R.; Sun, L., Photochemical hydrogen production catalyzed by polypyridyl ruthenium–cobaloxime heterobinuclear complexes with different bridges. *J. Organomet. Chem.* **2009,** *694*, 2814-2819.
20. Rupp, M.; Auvray, T.; Rousset, E.; Mercier, G. M.; Marvaud, V.; Kurth, D. G.; Hanan, G. S., Photocatalytic Hydrogen Evolution Driven by a Heteroleptic Ruthenium(II) Bis(terpyridine) Complex. *Inorg. Chem.* **2019,** *58*, 9127-9134.
21. Probst, B.; Rodenberg, A.; Guttentag, M.; Hamm, P.; Alberto, R., A Highly Stable Rhenium–Cobalt System for Photocatalytic H2 Production: Unraveling the Performance-Limiting Steps. *Inorg. Chem.* **2010,** *49*, 6453-6460.
22. Probst, B.; Guttentag, M.; Rodenberg, A.; Hamm, P.; Alberto, R., Photocatalytic H2 Production from Water with Rhenium and Cobalt Complexes. *Inorg. Chem.* **2011,** *50*, 3404-3412.

23. Yang, M.; Yarnell, J. E.; El Roz, K.; Castellano, F. N., A Robust Visible-Light-Harvesting Cyclometalated Ir(III) Diimine Sensitizer for Homogeneous Photocatalytic Hydrogen Production. *ACS Appl. Energy Mater.* **2020,** *3*, 1842-1853.
24. Lentz, C.; Schott, O.; Auvray, T.; Hanan, G.; Elias, B., Photocatalytic Hydrogen Production Using a Red-Absorbing Ir(III)–Co(III) Dyad. *Inorg. Chem.* **2017,** *56*, 10875-10881.
25. Takizawa, S.-y.; Katoh, S.; Okazawa, A.; Ikuta, N.; Matsushima, S.; Zeng, F.; Murata, S., Triplet Excited States Modulated by Push–Pull Substituents in Monocyclometalated Iridium(III) Photosensitizers. *Inorg. Chem.* **2021,** *60*, 4891-4903.
26. Jacques, A.; Schott, O.; Robeyns, K.; Hanan Garry, S.; Elias, B., Hydrogen Photoevolution from a Green-Absorbing Iridium(III)–Cobalt-(III) Dyad. *Eur. J. Inorg. Chem.* **2016,** *2016*, 1779-1783.
27. Bevernaegie, R.; Wehlin, S. A. M.; Piechota, E. J.; Abraham, M.; Philouze, C.; Meyer, G. J.; Elias, B.; Troian-Gautier, L., Improved Visible Light Absorption of Potent Iridium(III) Photo-oxidants for Excited-State Electron Transfer Chemistry. *J. Am. Chem. Soc.* **2020,** *142*, 2732-2737.
28. Tsuboyama, A.; Iwawaki, H.; Furugori, M.; Mukaide, T.; Kamatani, J.; Igawa, S.; Moriyama, T.; Miura, S.; Takiguchi, T.; Okada, S.; Hoshino, M.; Ueno, K., Homoleptic Cyclometalated Iridium Complexes with Highly Efficient Red Phosphorescence and Application to Organic Light-Emitting Diode. *J. Am. Chem. Soc.* **2003,** *125*, 12971-12979.
29. Nonoyama, M., Benzo[h]quinolin-10-yl-N Iridium(III) Complexes. *B. Chem. Soc. Jpn.* **1974,** *47*, 767-768.
30. Costa, R. n. D.; OrtÃ-, E.; Bolink, H. J.; Graber, S.; Schaffner, S.; Neuburger, M.; Housecroft, C. E.; Constable, E. C., Archetype Cationic Iridium Complexes and Their Use in Solid-State Light-Emitting Electrochemical Cells. *Advanced Functional Materials* **2009,** *19*, 3456-3463.
31. Lentz, C.; Schott, O.; Auvray, T.; Hanan, G. S.; Elias, B., Design and photophysical studies of iridium(iii)-cobalt(iii) dyads and their application for dihydrogen photo-evolution. *Dalton Trans* **2019,** *48*, 15567-15576.
32. Elgrishi, N.; Rountree, K. J.; McCarthy, B. D.; Rountree, E. S.; Eisenhart, T. T.; Dempsey, J. L., A Practical Beginner's Guide to Cyclic Voltammetry. *J. Chem. Ed.* **2018,** *95*, 197-206.
33. Brouwer, A., Standards for photoluminescence quantum yield measurements in solution (IUPAC Technical Report)*. *Pure and Applied Chemistry* **2011,** *83*.
34. Aydogan, A.; Bangle, R. E.; De Kreijger, S.; Dickenson, J. C.; Singleton, M. L.; Cauët, E.; Cadranel, A.; Meyer, G. J.; Elias, B.; Sampaio, R. N.; Troian-Gautier, L., Mechanistic investigation of a visible light mediated dehalogenation/cyclisation reaction using iron(iii), iridium(iii) and ruthenium(ii) photosensitizers. *Catalysis Science & Technology* **2021,** *11*, 8037-8051.
35. Lowry, M. S.; Bernhard, S., Synthetically Tailored Excited States: Phosphorescent, Cyclometalated Iridium(III) Complexes and Their Applications. *Chem-Eur. J.* **2006,** *12*, 7970-7977.
36. Lakowicz, J. R., *Principles of Fluorescence Spectroscopy*. Springer US, New York: 2006.
37. Rupp, M. T.; Auvray, T.; Shevchenko, N.; Swoboda, L.; Hanan, G. S.; Kurth, D. G., Substituted 2,4-Di(pyridin-2-yl)pyrimidine-Based Ruthenium Photosensitizers for Hydrogen Photoevolution under Red Light. *Inorg. Chem.* **2021,** *60*, 292-302.

38. Razavet, M.; Artero, V.; Fontecave, M., Proton Electroreduction Catalyzed by Cobaloximes: Functional Models for Hydrogenases. *Inorg. Chem.* **2005,** *44*, 4786-4795.
39. Jacques, P.-A.; Artero, V.; Pécaut, J.; Fontecave, M., Cobalt and nickel diimine-dioxime complexes as molecular electrocatalysts for hydrogen evolution with low overvoltages. *Proc. Natl. Acad. Sci. USA* **2009,** *106*, 20627-20632.
40. Xu, B.; Troian-Gautier, L.; Dykstra, R.; Martin, R. T.; Gutierrez, O.; Tambar, U. K., Photocatalyzed Diastereoselective Isomerization of Cinnamyl Chlorides to Cyclopropanes. *J. Am. Chem. Soc.* **2020,** *142*, 6206-6215.
41. Morton, C. M.; Zhu, Q.; Ripberger, H.; Troian-Gautier, L.; Toa, Z. S. D.; Knowles, R. R.; Alexanian, E. J., C–H Alkylation via Multisite-Proton-Coupled Electron Transfer of an Aliphatic C–H Bond. *J. Am. Chem. Soc.* **2019,** *141*, 13253-13260.
42. Four, P.; Guibe, F., Palladium-catalyzed reaction of tributyltin hydride with acyl chlorides. A mild, selective, and general route to aldehydes. *J. Org. Chem.* **1981,** *46*, 4439-4445.
43. Kober, E. M.; Caspar, J. V.; Lumpkin, R. S.; Meyer, T. J., Application of the energy gap law to excited-state decay of osmium(II)-polypyridine complexes: calculation of relative nonradiative decay rates from emission spectral profiles. *J. Phys. Chem* **1986,** *90*, 3722-3734.

For TOC use only

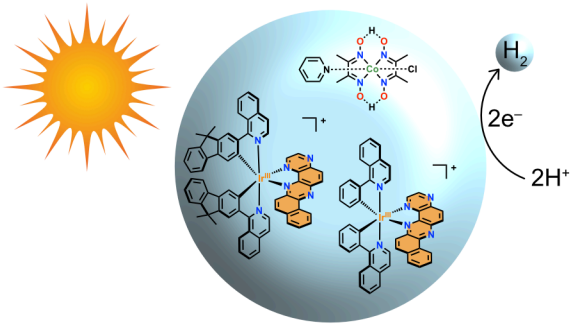

Two novel Iridium(III) photosensitizers were developed and used for the visible light induced hydrogen production using cobaloxime catalysts. Compared to prototypical $[Ir(ppy)_2(bpy)]^+$, these two Ir(III) photosensitizer presented increased visible light absorption (up to 634 nm) and displayed HER for more than 90 hours using blue, green and red irradiation wavelengths.